

Battery State of Health Estimation and Incremental Capacity Analysis for Charging with General Current Profiles Using Neural Networks

Qinan Zhou^{1,*}, Gabrielle Vuylsteke², R. Dyche Anderson², and Jing Sun³

Abstract—Incremental capacity analysis (ICA) and differential voltage analysis (DVA) conventionally require constant-current conditions for battery degradation monitoring, which restricts their applicability in real-world scenarios. This paper presents a unified approach to enable ICA/DVA-based degradation monitoring under general charging current profiles, which has not been addressed previously in the literature. First, a novel concept of virtual incremental capacity (IC) and different voltage (DV) is proposed. Second, two related convolutional neural networks (CNNs), called U-Net and Conv-Net, are proposed to construct virtual IC/DV curves and estimate the state of health (SOH) from general charging profiles across any state-of-charge (SOC) ranges that satisfy some constraints. Finally, two CNNs, called Mobile U-Net and Mobile-Net, are proposed to replace the U-Net and Conv-Net, respectively, for onboard implementations. They significantly reduce the computation and memory requirements, while retaining performance in virtual IC/DV curve construction and SOH estimation. Tested on an extensive experimental dataset of battery modules with various fast-charging protocols and SOC ranges, the proposed U-Net and Mobile U-Net construct accurate virtual IC/DV curves which enable the extraction of valuable degradation features. The proposed Conv-Net and Mobile-Net provide module-level SOH estimates with root-mean-square error (RMSE) of less than 0.5%.

Keywords—Incremental Capacity Analysis; Differential Voltage Analysis; Nonconstant-Current Charging; Fast Charging; Convolutional Neural Network; State of Health Estimation

LIST OF ACRONYMS

BMS	Battery Management System
CC	Constant Current
CNN	Convolutional Neural Network
DVA	Differential Voltage Analysis
ICA	Incremental Capacity Analysis
MSE	Mean Squared Error
NMC	Lithium Nickel-Manganese-Cobalt Oxide
PA	Partial Area
PH	Peak Height
RSME	Root-Mean-Square Error
SOC	State of Charge
SOH	State of Health

¹Qinan Zhou is with the Department of Mechanical Engineering, University of Michigan, Ann Arbor, MI 48103, USA. Email: qinan@umich.edu

²Gabrielle Vuylsteke and R. Dyche Anderson are with Research and Advanced Engineering, Ford Motor Company, Dearborn, MI 48124, USA. Email: {gvuylste, rander34}@ford.com

³Jing Sun is with the Department of Naval Architecture and Marine Engineering, University of Michigan, Ann Arbor, MI 48103, USA. Email: jingsun@umich.edu

*Corresponding Author.

I. INTRODUCTION

Battery state of health (SOH) and the associated degradation information are critical for range estimation, performance optimization, safe operation, maintenance, and warranty of electrified vehicles [1]. Estimating and monitoring SOH using onboard measurements are essential for battery management systems (BMS) [2]. The topic has been addressed extensively by the research and engineering communities. SOH can be characterized by either capacity fading or resistance rising, both of which lead to a reduction in usable energy [3], [4]. This paper focuses on capacity fading and defines SOH as $SOH = C/C_{\text{fresh}}$, where C and C_{fresh} are the capacities of a battery at its current and fresh state, respectively.

The battery degradation status can be accessed using intrusive and non-intrusive methods. Various intrusive methods, including photoelectron spectroscopy [5], scanning electron microscopy [6], X-ray diffraction [7], etc., provide the exact health and degradation status of batteries, but require expensive equipment and may lead to changes in battery performance or even cause permanent damage [3]. Thus, they are more suitable for laboratory testing. In contrast, non-intrusive methods use measurements such as current, voltage, and temperature to infer the battery degradation status. Popular non-intrusive methods include electrochemical impedance spectroscopy [8], incremental capacity analysis (ICA) [9], differential voltage analysis (DVA) [10], [11], adaptive filtering [12]–[14], and data-driven techniques [15], [16]. This paper focuses on ICA and DVA, as they do not require special instrumentation and can be implemented with existing onboard vehicle sensors.

In ICA/DVA, incremental capacity (IC) and differential voltage (DV) curves are obtained and, then, IC and DV features are extracted from these curves [17]. As changes in these features reveal certain aspects of degradation mechanisms within batteries [9], [18], one can correlate the IC/DV features and their changes with underlying degradation physics. Such an ability to provide physical insights into degradation without using complicated mechanistic models is the key strength of ICA/DVA over other data-driven or deep learning-based approaches for degradation monitoring.

ICA/DVA can be used in BMS for different applications, such as assessing remaining useful life [19] and detecting internal short-circuit faults [20]. One of their most important applications is SOH estimation. Data-driven methods are utilized to build models to relate IC/DV features with cell-level SOH under different charging conditions [17], [21]–

[24] and module-level SOH under cell-to-cell variations [25].

Despite all the advantages and applications, the primary limitation of ICA/DVA is that they are performed under constant-current (CC) charging [26]. In real-world applications, e.g. electrified vehicles, charging currents are non-constant, especially for fast charging [27] and constant-power charging. As a result, ICA/DVA-based degradation monitoring cannot be performed. Tang et al. attempted to extend ICA/DVA from CC charging to pulsed constant-current charging [28]. To the best of our knowledge, extending ICA/DVA to more general real-world charging current profiles has not been addressed by any paper in the literature.

This paper extends ICA/DVA to general charging profiles¹ by proposing a unified approach. For the first time, the proposed approach enables ICA/DVA-based SOH estimation and degradation monitoring without requiring constant-current conditions and broad state-of-charge (SOC) charging ranges. For performance assessment, a large experimental dataset of battery modules with three cells connected in parallel is used. Specifically, the contributions of the paper are four-fold:

- First, notions of virtual IC/DV curves and features are proposed. For cells or modules charged using general current profiles¹, virtual IC/DV curves are defined as the IC/DV curves that the same cells or modules, in the identical state of degradation, would exhibit under CC charging at a reference C-rate of interest. Features extracted from virtual IC/DV curves are defined as virtual IC/DV features. Virtual IC/DV curves and features reflect degradation mechanisms and can be used for SOH estimation, enabling ICA/DVA-based degradation monitoring for general charging profiles¹.
- Second, a convolutional neural network (CNN), called U-Net, constructs virtual IC/DV curves from general charging profiles with any SOC ranges satisfying some constraints. Applied to the aforementioned dataset, virtual IC/DV curves approximate actual IC/DV curves very well. As a case study of leveraging virtual IC/DV curves for SOH estimation, 0.6% root-mean-square error (RMSE) is achieved using only two extracted virtual IC/DV features.
- Third, by simplifying the architecture of U-Net, a CNN called Conv-Net is proposed to estimate SOH directly. For the same dataset, Conv-Net provides SOH estimates from general charging profiles with RMSE of 0.49% SOH.
- Fourth, for onboard implementations, two more computationally efficient CNNs, called Mobile U-Net and Mobile-Net, are developed to replace U-Net and Conv-Net, respectively. For the same dataset, the Mobile U-Net and Mobile-Net significantly reduce the computation and memory demands, with the number of parameters in neural networks being roughly 1/3 of U-Net

¹Hereafter, the term “general current profiles” refers to current profiles that are not necessarily constant, and the term “general charging profiles” denotes profiles that can be measured from charging with general current profiles, such as profiles of voltage, current, transferred charge, etc.

and Conv-Net, while keeping similar performance for virtual IC/DV curve construction and SOH estimation.

Therefore, the unified approach provides different aspects of ICA/DVA, including virtual IC/DV curves, virtual IC/DV features, and SOH estimates.

To elucidate the proposed approach, the paper is organized as follows. Section II defines virtual IC/DV curves and features. Section III describes the proposed U-Net and Mobile U-Net, while Section IV explains the proposed Conv-Net and Mobile-Net. Section V discusses the battery module dataset used in this study. Section VI assesses the performance of the proposed methods using the experimental data. Section VII summarizes the paper.

II. VIRTUAL INCREMENTAL CAPACITY AND DIFFERENTIAL VOLTAGE CURVES

This section defines the fundamental concepts that underpin this work. First, virtual IC/DV curves are defined. Then, virtual IC/DV features are briefly discussed.

IC/DV curves are originally defined in fully relaxed open-circuit conditions [9], which are rarely encountered in on-board BMS applications. To adapt to real-world scenarios, IC/DV curves are, later in the literature [17], [23], [29]–[31], defined as:

- **IC Curve:** $IC_{CC} = dQ_{CC}/dV_{CC}$ as a function of V_{CC} ,
- **DV Curve:** $DV_{CC} = dV_{CC}/dQ_{CC}$ as a function of Q_{CC} ,

where V_{CC} is voltage and Q_{CC} is the charged capacity under CC charging with a reference C-rate of interest. Note that the subscript “CC” is used here to emphasize that these quantities are obtained from the constant-current conditions and the shapes of IC/DV curves depend on the C-rate [32].

Consider cells or modules charged with general current profiles. Even though Q - V profiles can be measured and their derivatives can be computed, the obtained derivative curves are not meaningful for ICA/DVA purposes.

To overcome this limitation, this paper defines the virtual IC/DV curves as the IC/DV curves that the same cells or modules, in the identical state of degradation, would exhibit under CC charging at the same reference C-rate, denoted as:

- **Virtual IC Curve:** $\hat{I}C_{CC}$ as a function of \hat{V}_{CC} ,
- **Virtual DV Curve:** $\hat{D}V_{CC}$ as a function of \hat{Q}_{CC} ,

where \hat{V}_{CC} , \hat{Q}_{CC} , $\hat{I}C_{CC}$, and $\hat{D}V_{CC}$ are estimates constructed from measured general charging profiles. Note that the annotation $\hat{\cdot}$ is used to emphasize that they are estimates based on charging profiles that are not necessarily constant-current.

Features extracted from virtual IC/DV curves are called virtual IC/DV features and defined similarly to the corresponding actual IC/DV features defined in [9], [10], [18], [30], [33]. The specific virtual IC/DV features used in this paper are defined in Section V-A.

III. U-NET AND MOBILE U-NET FOR VIRTUAL IC/DV CURVE CONSTRUCTION

With key concepts defined, the next step is to develop a mapping from general charging profiles to virtual IC/DV

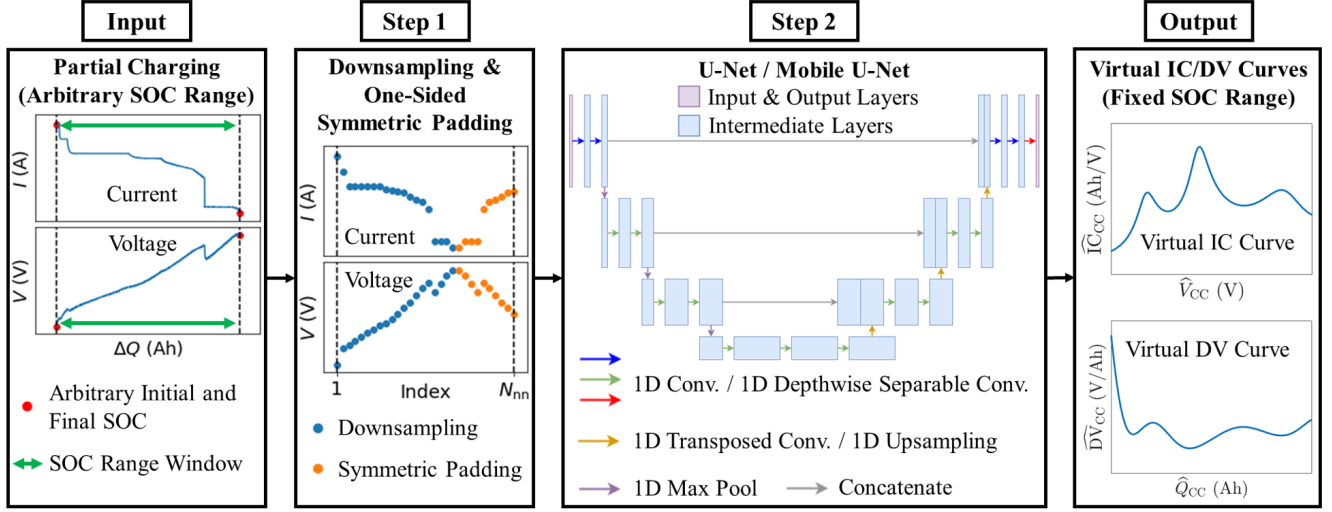


Fig. 1: Overview of Proposed Method for Virtual IC/DV Curve Construction

Algorithm 1: Proposed Method for Constructing Virtual IC and DV Curves (Fig. 1)

Output: $\{\hat{Q}_{cc}(k)\}$, $\{\hat{V}_{cc}(k)\}$, $\{\hat{I}_{cc}(k)\}$, $\{\hat{D}_{V_{cc}}(k)\}$

Input: $\{I(\Delta Q)\}$ and $\{V(\Delta Q)\}$ from general charging, a pre-stored increment Δq

$\{\tilde{I}(k)\}$, $\{\tilde{V}(k)\} \leftarrow$ Process $\{I(\Delta Q)\}$, $\{V(\Delta Q)\}$ using Algorithm 2

$\{\tilde{I}^{(s)}(k)\}$, $\{\tilde{V}^{(s)}(k)\} \leftarrow$ Equation (5)

$\{\hat{Q}_{cc}^{(s)}(k)\}$, $\{\hat{V}_{cc}^{(s)}(k)\}$, $\{\hat{I}_{cc}^{(s)}(k)\} \leftarrow$ U-Net/Mobile U-Net($\{\tilde{I}^{(s)}(k)\}$, $\{\tilde{V}^{(s)}(k)\}$)

$\{\hat{Q}_{cc}(k)\}$, $\{\hat{V}_{cc}(k)\}$, $\{\hat{I}_{cc}(k)\} \leftarrow$ Equation (5)

$\{\hat{D}_{V_{cc}}(k)\} \leftarrow 1/\{\hat{I}_{cc}(k)\}$

$/* \Delta Q \in [0, \overline{\Delta Q}]$, $k \in \{1, 2, \dots, N_{nn}\}$

$*/$

curves so that ICA/DVA can be performed. Because such a mapping is complicated to formulate, a CNN-based approach is adopted. This section elaborates on the proposed method shown in Fig. 1. The main components of the proposed method in Fig. 1 are the U-Net and Mobile U-Net in Step 2, while Step 1 ensures that inputs to the CNNs are properly prepared. The overall procedure of the proposed method is also summarized in Algorithm 1.

Compared to other CNNs, U-Net is chosen for two reasons. First, its encoder-decoder structure provides a clear separation between feature extraction and profile construction, which leads to better explainability [34]. Second, its skip connections preserve spatial information at both local and global levels and allow the neural network to optimally integrate such information for profile construction [35].

Inspired by [36], this paper derives a more computationally efficient CNN called Mobile U-Net to replace U-Net for on-board implementations. By modifying layers and keeping the architecture of U-Net, Mobile U-Net reduces computational and memory requirements significantly, without compromising performance in virtual IC/DV curve construction.

The details of the proposed method in Fig. 1 and the training of the proposed CNNs are explained in the following subsections.

A. Input

Define $SOC_{initial}$, SOC_{final} , $\Delta SOC = SOC_{final} - SOC_{initial}$ as initial SOC, final SOC, and partial charging range, respectively. Consider a general charging event with a charging SOC range falling in the following SOC window:

$$\begin{cases} SOC_{initial} \leq \overline{SOC}_{initial} \\ SOC_{final} \geq \underline{SOC}_{final} \\ \Delta SOC \geq \underline{\Delta SOC} \end{cases}, \quad (1)$$

where the underline $\underline{\cdot}$ and overline $\overline{\cdot}$ represent the lower and upper bounds for corresponding variables, respectively. Note that a minimum SOC window is needed for the proposed method, because charging profiles need to contain sufficient information for constructing virtual IC/DV curves properly.

Let $\{I(t)\}$, $\{V(t)\}$, $\{\Delta Q(t)\}$, $t \in [0, T]$ be the profiles of current, voltage, and transferred charge from the charging,

Algorithm 2: Proposed Downsampling and One-Sided Symmetric Padding Algorithm

Output: downsampled and symmetrically padded current $\{\tilde{I}(k)\}$ and voltage $\{\tilde{V}(k)\}$

Input: current $\{I(\Delta Q)\}$, voltage $\{V(\Delta Q)\}$, a pre-stored increment Δq

$\{\tilde{I}(\Delta Q)\}, \{\tilde{V}(\Delta Q)\} \leftarrow$ Downsample current and voltage so that there is one datapoint every Δq
 $\{\tilde{I}(k)\}, \{\tilde{V}(k)\} \leftarrow$ One-sided symmetrically pad $\{\tilde{I}(\Delta Q)\}$ and $\{\tilde{V}(\Delta Q)\}$ until N_{nn} points

$/ * \Delta Q \in [0, \overline{\Delta Q}], k \in \{1, 2, \dots, N_{\text{nn}}\}$

$*/$

respectively, where t is time and T is the total charging time. The transferred charge is defined as:

$$\Delta Q(t) = \int_0^t I(\tau) d\tau \in [0, \overline{\Delta Q}]. \quad (2)$$

$\{\Delta Q(t)\}$ always starts at 0 and ends at the total amount of transferred charge ($\overline{\Delta Q}$). Furthermore, both $\{I(t)\}$ and $\{V(t)\}$ can be re-written as functions of $\{\Delta Q(t)\}$, denoted as $\{I(\Delta Q)\}, \{V(\Delta Q)\}, \Delta Q \in [0, \overline{\Delta Q}]$, respectively.

The inputs to the proposed method in Fig. 1 are $\{I(\Delta Q)\}$ and $\{V(\Delta Q)\}$. Hence, the proposed method does not use SOC as an input.

B. Downsampling and One-Sided Symmetric Padding

$\{I(\Delta Q)\}$ and $\{V(\Delta Q)\}$ profiles measured onboard, even for a limited SOC range, typically have different profile lengths and a lot more datapoints than the number of datapoints required by the proposed CNNs. Thus, downsampling and one-sided symmetric padding in Step 1 of Fig. 1 are used to prepare the input signals to a standard format, as implemented in Algorithm 2.

This paper proposes to downsample profiles based on transferred charge (ΔQ) for the following reasons. First, time-based downsampling does not capture the most important information to represent a charging profile. For example, in fast charging, charging from 80% to 100% SOC takes a significant portion of the charging time because of low current magnitude [27], and therefore has the most number of the datapoints after downsampling. However, this only covers a small portion of the charging range. Second, downsampling based on SOC or ΔQ will overcome the limitations of time-based downsampling, but SOC needs to be estimated in practice [37], and using estimates brings additional uncertainty to the proposed method. Thus, downsampling based on ΔQ is the most suitable.

Specifically, $\{I(\Delta Q)\}$ and $\{V(\Delta Q)\}$ are downsampled for every incremental Δq defined as:

$$\Delta q = \frac{\Delta Q_{\text{max}}}{N_{\text{nn}}}, \quad (3)$$

where N_{nn} is the number of datapoints required by the proposed CNNs, and ΔQ_{max} is the maximum amount of transferred charge the proposed method needs to handle. One way to determine ΔQ_{max} is:

$$\Delta Q_{\text{max}} = \overline{\Delta \text{SOC}} \cdot C_{\text{fresh}}, \quad (4)$$

where $\overline{\Delta \text{SOC}}$ is the maximum charging SOC range to be handled, and C_{fresh} is the capacity of a battery at the fresh state. Note that ΔQ_{max} and Δq only need to be computed once at the calibration phase of the proposed algorithm and stored in the algorithm. Hence, the proposed downsampling algorithm does not require any SOC information at the deployment phase.

Remark 1. The total amount of transferred charge $\overline{\Delta Q}$ in $\{I(\Delta Q)\}$ and $\{V(\Delta Q)\}$ profiles is not necessarily divisible by Δq . Thus, after downsampling, each original profile often has a small remainder portion with the amount of transferred charge less than Δq . Because Δq is chosen to be small, this remainder can be omitted for the rest of the proposed method.

Note that, because profiles have different $\overline{\Delta Q}$ originally, the number of datapoints in downsampled profiles (N_{point}) is different for different profiles and smaller than the required number of datapoints by the proposed CNNs (N_{nn}). This is the consequence of making downsampled profiles have the same measurement frequency in the Δq -domain, which is required as CNN filters have fixed kernel sizes [34]. Thus, padding is adopted to meet the dimension requirement.

While there are many different padding methods [38], this paper adopts and modifies the symmetric padding proposed by [39] because of its ability to reduce construction errors at the borders of the constructed profiles. Specifically, this paper performs the one-sided symmetric padding, which adds mirrored datapoints to the end of the target profile until the desired length is reached. For example, if one wants to pad the profile array $[a, b, c]$ to have 8 points in length, then one keeps these three points at the beginning (left side) of the array and then adds additional mirrored points at the end (right side). The resulting padded array is $[a, b, c, c, b, a, a, b]$. For any downsampled profiles with N_{point} points, they will be one-sided symmetrically padded to have N_{nn} points by adding $(N_{\text{nn}} - N_{\text{point}})$ points at the end (right side).

After these two steps of processing, the resulting current and voltage profiles, denoted as $\{\tilde{I}(k)\}, \{\tilde{V}(k)\}, k \in \{1, 2, \dots, N_{\text{nn}}\}$, respectively, are sent as two separate channels to the proposed CNNs, where k is an index. ΔQ profile is no longer needed, as it is implicitly embedded in the downsampled current and voltage profiles.

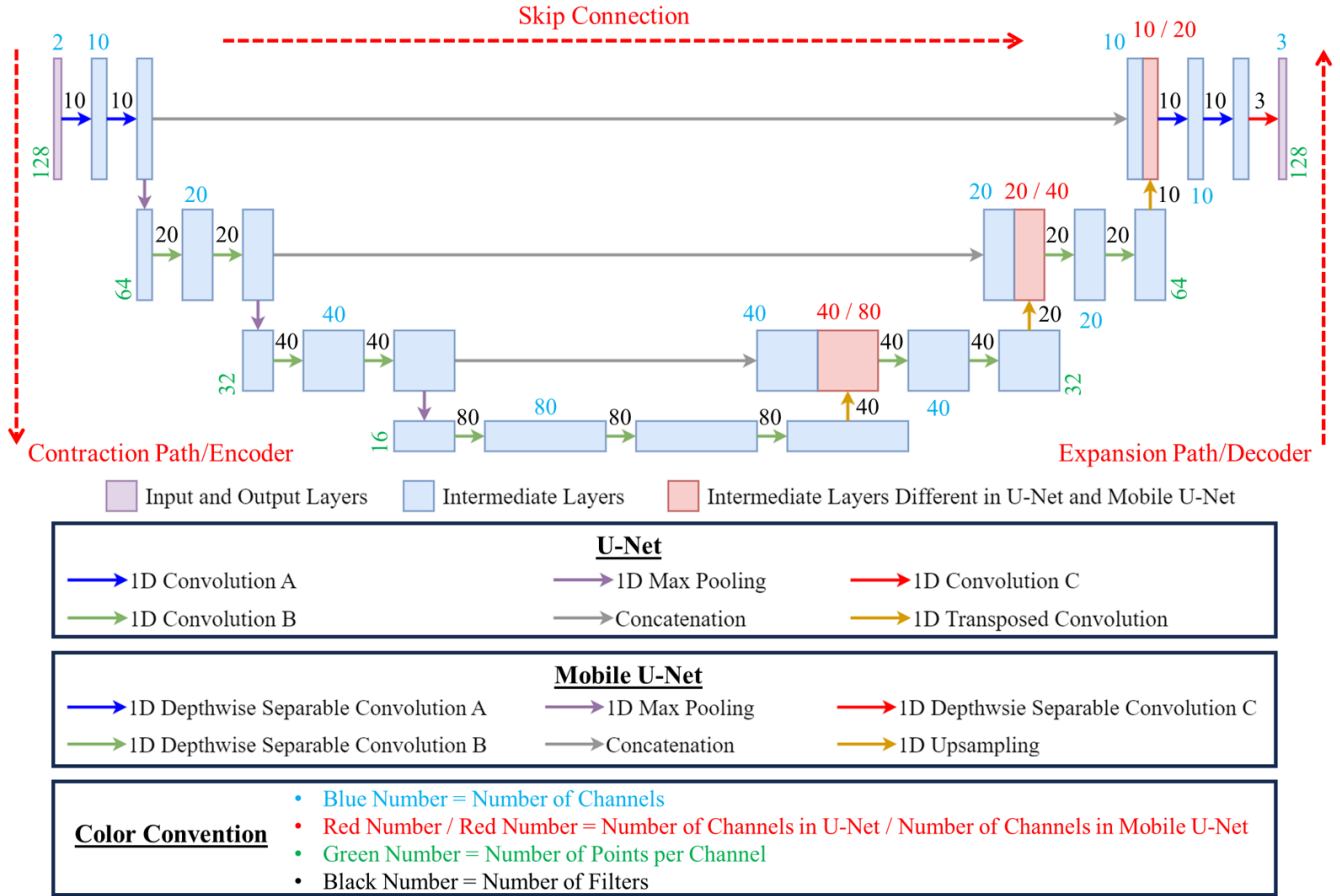


Fig. 2: Proposed U-Net and Mobile U-Net for Constructing Virtual IC/DV Curves

C. Output

The outputs of Fig. 1 contain three separate channels, namely $\{\widehat{Q}_{CC}(k)\}$, $\{\widehat{V}_{CC}(k)\}$, $\{\widehat{I}_{CC}(k)\}$, $k \in \{1, 2, \dots, N_{nn}\}$. $\{\widehat{D}_{V_{CC}}(k)\}$ is obtained using $\widehat{D}_{V_{CC}}(k) = 1/\widehat{I}_{CC}(k)$. The SOC range of the outputs is fixed and the same, no matter what SOC ranges the inputs have. The fixed SOC range does not need to be full-range and just needs to be broad enough to encompass all the IC/DV features of interest. This paper denotes this fixed SOC range as $\widehat{SOC} \in [\widehat{SOC}_{initial}, \widehat{SOC}_{final}]$. Furthermore, datapoints are evenly distributed from $\widehat{SOC}_{initial}$ to \widehat{SOC}_{final} for $\{\widehat{Q}_{CC}(k)\}$, $\{\widehat{V}_{CC}(k)\}$, $\{\widehat{I}_{CC}(k)\}$ profiles. Also, due to the symmetry of the U-Net architecture (to be discussed in Sections III-D and III-E), the number of datapoints for the outputs is the same as the inputs and equal to N_{nn} .

D. Overview of U-Net and Mobile U-Net

This subsection elaborates on the intuitions and working mechanisms of U-Net and Mobile U-Net used in Step 2 of Fig. 1. The proposed U-Net and Mobile U-Net are shown in Fig. 2. The software package Keras [40] is used to build, train, validate, and test the proposed CNNs.

The U-Net shown in Fig. 2 consists of three main

components, namely the contraction path, skip connections, and expansion path [41]. The contraction path (or encoder) consists of convolution and max pooling [34]. The purpose of the contraction path is to extract features at different levels. As the neural network goes deeper into the contraction path (following the direction of the dashed red arrow in Fig. 2), more global and less local features are extracted [42]. The skip connections, i.e., concatenations shown in Fig. 2, send the extracted features to the expansion path and allow the neural network to leverage both local and global features for profile constructions [35]. The expansion path (or decoder) consists of convolution and transposed convolution [34]. The purpose of the expansion path is to construct profiles using received features. During the construction phase, transposed convolution finds an optimal way to expand dimensions and increase resolutions of constructed profiles, while convolution combines the constructed profiles with received features [41]. Finally, as a result of these main components, the U-Net has a symmetric architecture and forms the shape of ‘‘U’’.

For onboard implementations, the computational and memory demands of the proposed U-Net can be further reduced without compromising performance. Thus, Mobile U-Net is proposed. The Mobile U-Net in Fig. 2 has the same architecture as the proposed U-Net, but uses different layers. First, depthwise separable convolution is used to replace

TABLE I: Summary of Settings for Proposed U-Net and Conv-Net

Layers	Settings	
1D Convolution	Number of Filters	Varies, Numbers Given in Fig. 2 and Fig. 4 in Black
	Kernel Size	(A): 11 (B): 3 (C): 11 for U-Net, 3 for Conv-Net
	Stride	1
	Padding	Same-Padding Strategy
	Parameter Initializer	He Normal
	Bias Used	(A): False (B): False (C): True
	Batch Normalization	(A): Applied After Linear Operation and Before Nonlinear Activation (B): Applied After Linear Operation and Before Nonlinear Activation (C): None
	Activation Function	(A): Parametric ReLU with Shared Axis = Axis 1* (B): Parametric ReLU with Shared Axis = Axis 1* (C): None
1D Transposed Convolution	Number of Filters	Varies, Numbers Given in Fig. 2 and Fig. 4 in Black
	Kernel Size	3
	Stride	2
	Padding	Same-Padding Strategy
	Parameter Initializer	He Normal
	Bias Used	False
	Batch Normalization	Applied After Linear Operation and Before Nonlinear Activation
	Activation Function	Parametric ReLU with Shared Axis = Axis 1*
1D Max Pooling	Pool Size	2
Concatenation	Concatenation Axis	Axis 2*

* Array Format of Proposed Neural Networks: (Axis 0, Axis 1, Axis 2) = (Batch Size, Profile Length, Number of Channels).

TABLE II: Summary of Settings for Proposed Mobile U-Net and Mobile-Net

Layers	Settings	
1D Depthwise Separable Convolution	Number of Filters (in Pointwise Convolution)	Varies, Numbers Given in Fig. 2 and Fig. 4 in Black
	Kernel Size (in Depthwise Convolution)	(A): 11 (B): 3 (C): 11 for Mobile U-Net, 3 for Mobile-Net
	Stride	1
	Padding	Same-Padding Strategy
	Parameter Initializer	He Normal for Both Depthwise and Pointwise Convolutions
	Bias Used	(A): False (B): False (C): True
	Batch Normalization	(A): Applied After Linear Operation and Before Nonlinear Activation (B): Applied After Linear Operation and Before Nonlinear Activation (C): None
	Activation Function	(A): Parametric ReLU with Shared Axis = Axis 1* (B): Parametric ReLU with Shared Axis = Axis 1* (C): None
1D Upsampling	Size	2
1D Max Pooling	Pool Size	2
Concatenation	Concatenation Axis	Axis 2*

* Array Format of Proposed Neural Networks: (Axis 0, Axis 1, Axis 2) = (Batch Size, Profile Length, Number of Channels).

convolution. Depthwise separable convolution is proposed in [36] and widely used in various CNNs [36], [43]–[45] for mobile and embedded applications. It contains a depthwise convolution followed by a pointwise convolution, where the former performs filtering and the latter combines the filtered results [36]. Based on [36], the computation and memory reduction is significant, when switching from convolution to depthwise separable convolution. Second, upsampling with simple repetition from Keras [40] is used to replace transposed convolution. Such upsampling has no parameters to be learned. Thus, compared to transposed convolution, upsampling reduces the computation and memory signifi-

cantly, but loses the ability to learn an optimal way for expanding dimensions and increasing resolutions. A more detailed discussion about the computation and memory for U-Net and Mobile U-Net will be given in Section VI-D.

E. Specific Designs of U-Net and Mobile U-Net

U-Net and Mobile U-Net offer a high degree of design freedom, including the number of levels and layers per level in contraction and expansion paths. Fig. 2 shows the specific design used by this paper. Furthermore, every layer can be customized. Tables I and II summarize the detailed settings used for the proposed U-Net and Mobile U-Net, respectively.

Algorithm 3: Proposed Method for Constructing SOH Estimates (Fig. 3)

Output: SOH estimate $\widehat{\text{SOH}} \in [0, 1]$

Input: $\{I(\Delta Q)\}$ and $\{V(\Delta Q)\}$ from general charging, a pre-stored increment Δq

$\{\tilde{I}(k)\}, \{\tilde{V}(k)\} \leftarrow$ Process $\{I(\Delta Q)\}, \{V(\Delta Q)\}$ using Algorithm 2

$\{\tilde{I}^{(s)}(k)\}, \{\tilde{V}^{(s)}(k)\} \leftarrow$ Equation (5)

$\widehat{\text{SOH}} \leftarrow$ Conv-Net/Mobile-Net($\{\tilde{I}^{(s)}(k)\}, \{\tilde{V}^{(s)}(k)\}$)

$/ * \Delta Q \in [0, \overline{\Delta Q}], k \in \{1, 2, \dots, N_{\text{nn}}\}$

$*/$

For layer design, while some settings are directly adopted from [41], some are customized to fit the needs of this study and are worthy of discussion.

- **Performance Enhancement:** Kernel size and activation function are designed for better construction performance. Larger kernel sizes are used in “1D convolution A” and “1D depthwise separable convolution A” (defined in Fig. 2) to filter out input noises in the contraction path and generate smoother profiles in the expansion path. Parametric rectified linear unit (PReLU) [46] is used for activation. It learns optimal leakage hyperparameters to solve the dying ReLU problem, thereby leading to better performance without an increase in computational complexity [46]. Following [46], the PReLU used by this paper has one leakage hyperparameter shared within a channel and has different leakage hyperparameters across different channels.
- **Improved Training Efficiency:** He Normal parameter initialization [46] and batch normalization [47] are used to mitigate vanishing gradient problems during the training process [48]. Following [47], batch normalization is applied after linear operations and before nonlinear activations to remove the effects of biases in linear operations. Default hyperparameters for batch normalization in Keras [40] are adopted.

F. Standardization and Training

To make the training process unbiased and converge faster, the input profiles ($\{\tilde{I}(k)\}, \{\tilde{V}(k)\}$) and output profiles ($\{\widehat{Q}_{\text{CC}}(k)\}, \{\widehat{V}_{\text{CC}}(k)\}, \{\widehat{\text{IC}}_{\text{CC}}(k)\}$) are standardized first by using

$$\{z^{(s)}(k)\} = \frac{\{z(k)\} - \mu_z}{\sigma_z}, \quad (5)$$

where z can be any variable, e.g., \tilde{I} , \tilde{V} , \widehat{Q}_{CC} , \widehat{V}_{CC} , and $\widehat{\text{IC}}_{\text{CC}}$. μ_z and σ_z are the mean and standard deviation computed over all the points in all the training samples as:

$$\mu_z = \text{mean} \left(\left\{ \left[\{z(k)\}_j \right]_{j=1}^N \right\} \right), \quad (6)$$

$$\sigma_z = \text{std} \left(\left\{ \left[\{z(k)\}_j \right]_{j=1}^N \right\} \right), \quad (7)$$

where $\left[\{z(k)\}_j \right]$ represents the profile $\{z(k)\}$ from the j -th training sample, $k \in \{1, 2, \dots, N_{\text{nn}}\}$, and N is the total number of training samples.

The mean squared error (MSE) loss function from Keras [40] is used in this paper. The ADAM solver [49] with default settings in Keras [40] is used to solve the optimization problem, allowing adaptive learning rate, faster convergence, and bias corrections during the training process. As a regularization technique, early stopping is used to halt the training process when the validation MSE loss does not decrease for consecutive N_{th} epochs [48].

IV. CONV-NET AND MOBILE-NET FOR SOH ESTIMATION

With the trained U-Net and Mobile U-Net, virtual IC/DV curves can be constructed and the virtual IC/DV features can be extracted. The U-Net and Mobile U-Net can be simplified to provide SOH estimates directly from general charging profiles with any SOC ranges satisfying Constraint (1). The simplified CNNs are called Conv-Net and Mobile-Net.

There is a rich literature on CNNs for SOH estimation, e.g. [15], [50], [51]. Most use fully connected layers to achieve accurate SOH estimation, but fully connected layers have a significant number of parameters and require very large computational resources. Compared to these methods in the literature, the advantage of the proposed Conv-Net is that it contains only convolutions with significantly fewer parameters, thereby providing a substantial computational advantage. Then, for mobile and embedded applications, Mobile-Net is proposed to replace the Conv-Net, with even simpler computations and less memory requirements, while maintaining SOH estimation performance. A more detailed discussion about the computation and memory for Conv-Net and Mobile-Net will be given in Section VI-D.

The proposed method is shown in Fig. 3. The input, downsampling, and one-sided symmetric padding are the same as what is discussed in Sections III-A and III-B. The outputs are SOH estimates ranging from 0 to 1. The overall procedure of the proposed method is summarized in Algorithm 3.

The designed Conv-Net and Mobile-Net are shown in Fig. 4. It should be noted that one can train the proposed Conv-Net and Mobile-Net from scratch independently from the U-Net and Mobile U-Net. However, to have a unified

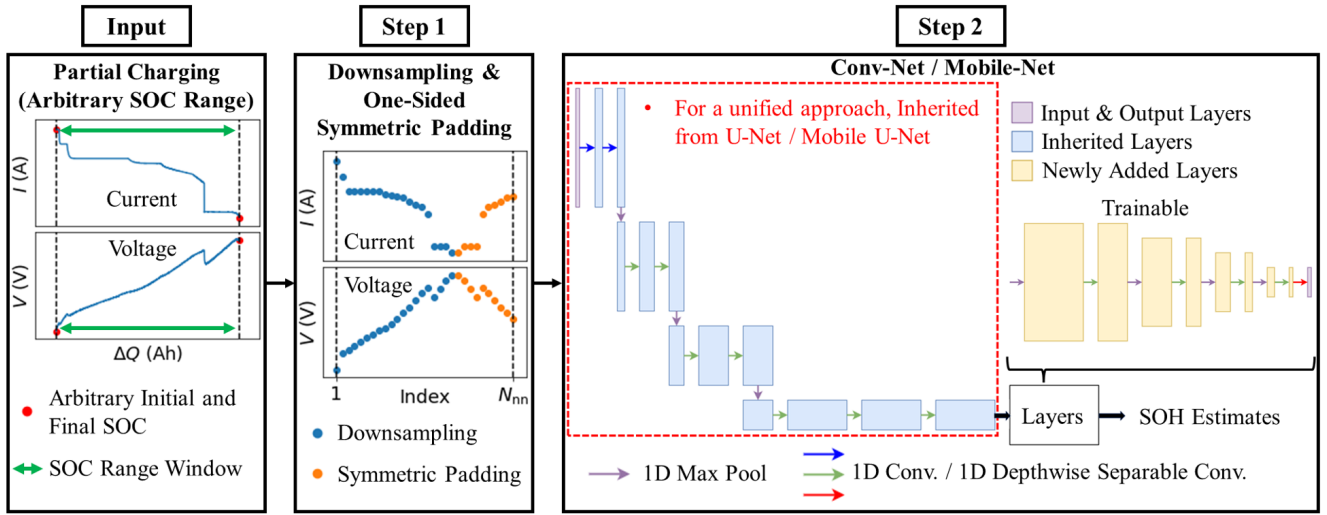


Fig. 3: Overview of Proposed Method for State of Health (SOH) Estimation

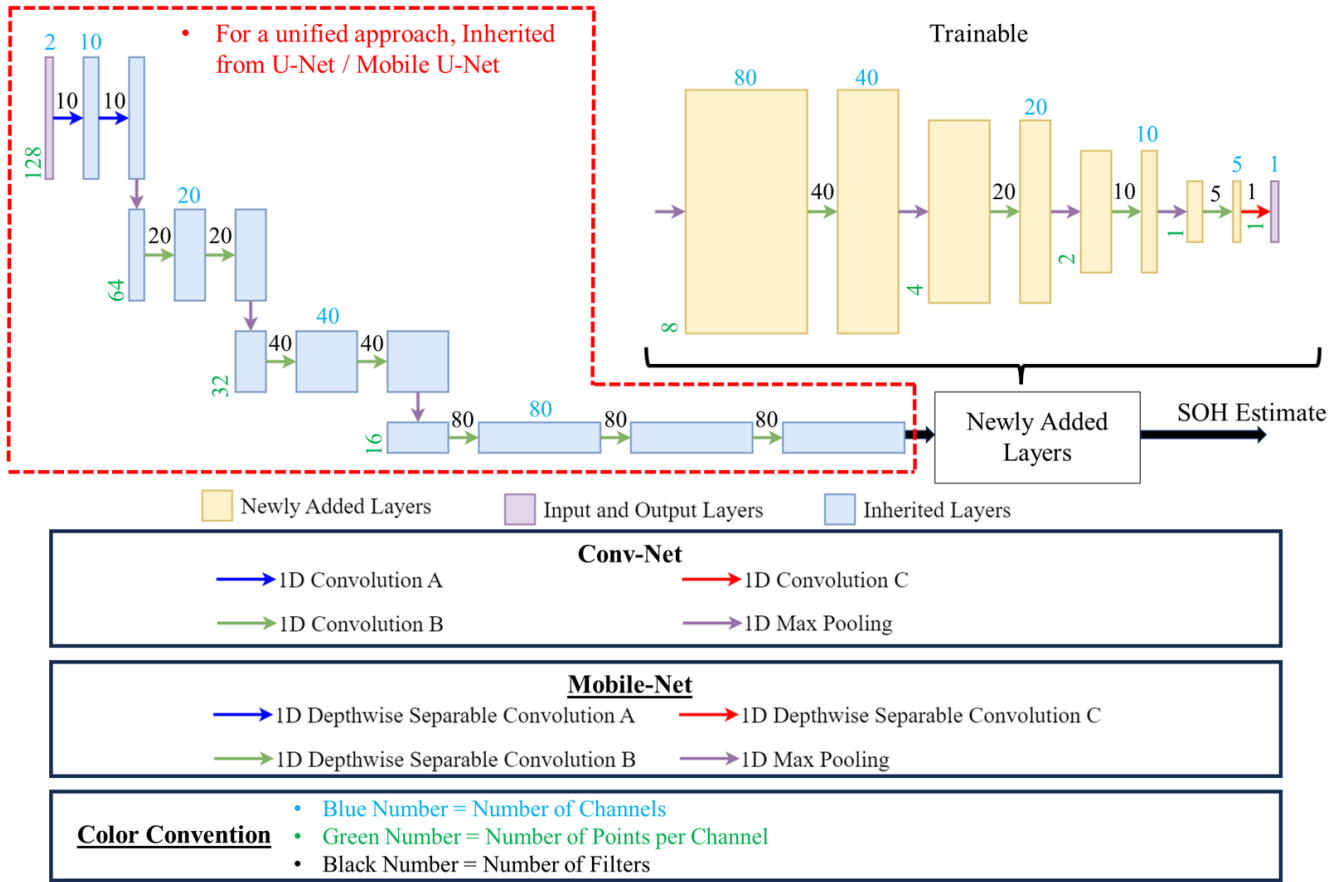


Fig. 4: Proposed Conv-Net and Mobile-Net for Estimating State of Health (SOH)

approach for virtual IC/DV curves, virtual IC/DV features, and SOH estimates, transfer learning is utilized here. Specifically, the entire contraction path of the trained U-Net and Mobile U-Net is transferred to the Conv-Net and Mobile-Net, respectively, for feature extraction. For the intuition behind this, features extracted from the contraction path are used to construct virtual IC/DV curves and, thus, contain

degradation information that can be leveraged to construct SOH estimates directly. The parameters associated with the contraction path are fixed during the training of the Conv-Net and Mobile-Net. New trainable layers of convolution or depthwise separable convolution are attached after the contraction path for regression purposes. Tables I and II summarize the settings used for the proposed Conv-Net and

Mobile-Net, respectively. The design logic is the same as what is discussed in Section III-E.

Similar to Section III-F, the MSE loss, ADAM solver [49], and early stopping are used for training. Since SOH takes values from 0 to 1, no additional standardization step is needed for outputs of the Conv-Net and Mobile-Net. In contrast, inputs to the Conv-Net and Mobile-Net should still be standardized using Equation (5) for faster convergence.

V. BATTERY DATASETS FOR EVALUATION

This section describes the battery module dataset used by this study for performance evaluation. Note that, given a charging profile with a specific charging SOC range, one can randomly truncate the profile to have different profiles with different charging SOC ranges.

A. Original Battery Dataset

The performance of the proposed unified approach delineated in Fig. 1 and Fig. 3 is demonstrated using a large experimental dataset of battery modules. Table III summarizes the key attributes of the dataset.

TABLE III: Key Attributes of the Battery Dataset

Attributes	Descriptions
Chemistry	NMC622
Module Nominal Capacity	208Ah
Module Configuration	3 Cells in Parallel
No. of Modules	96
Module-Level SOH Range	100% - 86%
No. of Fast Charging Protocols	3
No. of Input-Output Pairs	40512
No. of Input-Output Pairs Derived by Truncating	405120

Specifically, a proprietary dataset of lithium nickel-manganese-cobalt oxide 622 (NMC622) modules is used. 96 NMC622 modules consist of three NMC622 cells connected in parallel. These NMC622 modules are cycled using low C-rate charging profiles and fast charging profiles alternately. The low C-rate charging profile consists of two CC charging regimes with 86A and 64.5A module-level currents, respectively, and one subsequent constant-voltage regime. The module-level IC/DV curves are obtained using the first CC regime, as it contains all the module-level IC/DV features for this dataset. Three types of fast-charging protocols, as shown in Fig. 5, are used in this dataset, which improves the generalizability of the proposed CNNs.

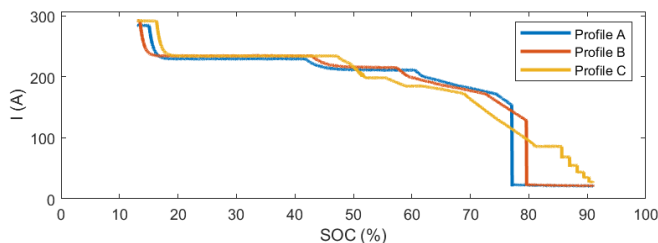


Fig. 5: Examples of Fast-Charging Current Profiles in the Dataset

Fig. 6 shows one example of module-level IC/DV curves. Features such as IC peak height (IC PH) and IC partial areas (IC PA) are used in this paper. As shown in Fig. 6, the IC PH is defined as the y -coordinate of the IC peak, and the IC PA is defined as the area either above a user-defined horizontal cutoff line (IC PA 2) or within a user-defined symmetric voltage window around a target IC peak (IC PA 1) [30].

For the training of the proposed U-Net and Mobile U-Net, the IC/DV curves from one low C-rate charging cycle are used as the ground truth for the outputs, while the fast charging profiles from the next cycle are used as inputs.

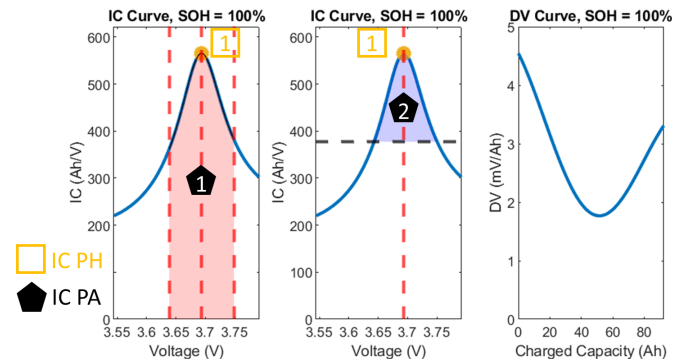


Fig. 6: Example Module-Level IC/DV Curves and Related IC/DV Features in the Dataset

B. Dataset Used for Training, Validation, and Testing of Proposed Neural Networks

The original dataset only contains one wide SOC range for fast charging, namely 13%-91% SOC. To develop, train, validate, and test the proposed methods under any charging SOC ranges that satisfy Constraint (1), the fast-charging profiles in the original dataset are randomly truncated to have different SOC ranges.

One example SOC window described by Constraint (1) can be: $SOC_{\text{initial}} \leq 50\%$, $SOC_{\text{final}} \geq 75\%$, and $\Delta SOC \geq 40\%$. Note that this window is chosen as an example and it can be varied depending on applications. Most importantly, a minimum SOC window is required, because the charging range has to be long enough to contain sufficient information for constructing virtual IC/DV curves and SOH estimates properly, as discussed in Section III-A. Furthermore, for this dataset, $\overline{\Delta SOC} = 91\% - 13\% = 78\%$. Then, with N_{nn} set in Section VI, ΔQ_{max} and Δq for the downsampling discussed in Section III-B are determined using Equations (3) and (4).

When truncating a given profile to obtain different SOC ranges, randomness is required to enable the trained CNNs to handle any SOC ranges within the specified SOC window. Assuming all different SOC ranges are equally important, the sampling distribution should be a uniform distribution satisfying Constraint (1). The Dirichlet-rescale algorithm proposed by [52] is used to generate random SOC ranges from such a constrained uniform distribution. In this case study, each input profile from the original dataset is truncated into 10 profiles with different random SOC ranges. The

number “10” is chosen empirically. The number of input-output pairs after random truncations is given in Table III.

VI. PERFORMANCE OF PROPOSED METHOD

This section evaluates the performance of the proposed CNNs using the dataset described in Section V-B. The dataset containing inputs with random SOC ranges that satisfy constraints given in Section V-B is randomly split into 60% training, 20% validation, and 20% testing sets for developments and evaluations. The comparisons among proposed U-Net, Mobile U-Net, Conv-Net, and Mobile-Net are elucidated. $N_{nn} = 128$ for the proposed CNNs, downsampling, and one-sided symmetric padding in Sections III and IV. The value of N_{nn} is a design choice that can be determined through trial and error. Lower N_{nn} reduces computation and memory requirements, while higher N_{nn} enhances the resolution of virtual IC/DV curves. The optimal value can be determined to balance the trade-off.

A. Accuracy of Constructed Virtual IC/DV Curves

This subsection examines the accuracy of virtual IC/DV curve construction and compares the performance of U-Net and Mobile U-Net.

Recall that outputs of the proposed U-Net and Mobile U-Net are standardized virtual profiles, $\{\hat{Q}_{CC}^{(s)}(k)\}$, $\{\hat{V}_{CC}^{(s)}(k)\}$, $\{\hat{IC}_{CC}^{(s)}(k)\}$, which are estimates for standardized actual curves, $\{Q_{CC}^{(s)}(k)\}$, $\{V_{CC}^{(s)}(k)\}$, $\{IC_{CC}^{(s)}(k)\}$. The metric to evaluate each constructed virtual IC/DV curve is defined as:

$$\text{Error} = \frac{1}{N_{nn}} \sum_{k=1}^{N_{nn}} \left\| \begin{bmatrix} IC_{CC}^{(s)}(k) \\ V_{CC}^{(s)}(k) \\ Q_{CC}^{(s)}(k) \end{bmatrix} - \begin{bmatrix} \hat{IC}_{CC}^{(s)}(k) \\ \hat{V}_{CC}^{(s)}(k) \\ \hat{Q}_{CC}^{(s)}(k) \end{bmatrix} \right\|_2, \quad (8)$$

where $\|\cdot\|_2$ is the Euclidean norm.

Fig. 7a shows the defined error distribution of the testing set under random input SOC ranges, divided into four categories. For each category, a pair of virtual and actual IC/DV curves from Mobile U-Net with an average error is shown in the rest of Fig. 7. Based on Fig. 7, there are several observations. First, most virtual IC/DV curves are close to their corresponding actual IC/DV curves. Therefore, the U-Net and Mobile U-Net can successfully construct virtual IC/DV curves with a fixed SOC range that covers all important IC/DV features. As a result, by using the U-Net and Mobile U-Net, one can perform ICA/DVA-based degradation monitoring under general charging, which cannot be done previously in the literature. Second, by comparing the error distributions of U-Net and Mobile U-Net in Fig. 7a, the Mobile U-Net has similar performance for virtual IC/DV curve construction, but reduces the computation and memory significantly (to be discussed in Section VI-D).

To show how well the U-Net and Mobile U-Net trained from random input SOC ranges perform when they are used in specific input SOC ranges, this paper investigates three cases, namely long-range (15%-90% SOC), medium-range (30%-80% SOC), and short-range (45%-90% SOC) fast

charging. Data for these three cases are obtained by directly truncating the original dataset. The U-Net and Mobile U-Net trained from random input SOC ranges are not re-trained for any specific ranges, and all the data from specific ranges are used for testing. Fig. 8 shows how error distributions from different specific ranges compared to the error distribution from random input ranges. Based on Fig. 8, the performance of the virtual IC/DV curve construction at specific input SOC ranges stays similar to the random input SOC range, but slightly deteriorates as the input SOC range decreases, because a shorter SOC range contains less information for virtual IC/DV curve construction.

In summary, the U-Net and Mobile U-Net trained from random input SOC ranges can be used directly without re-training for fast charging with any specific SOC ranges that satisfy constraints given in Section V-B.

B. Applications of Virtual IC/DV Curves and Features

To demonstrate that the constructed virtual IC/DV curves can be used for various degradation monitoring tasks, this paper uses module-level SOH estimation as a case study.

TABLE IV: Module-Level SOH Estimation Performance Using Virtual IC/DV Features

Neural Network	Charging Scheme	Test RMSE	Average Three-Sigma Value	No. of Relevance Vectors
-	CC	0.53% SOH	1.56% SOH	7
U-Net	Fast	0.60% SOH	1.74% SOH	6
Mobile U-Net	Fast	0.61% SOH	1.77% SOH	8

For module-level SOH estimation, an optimal set of IC/DV features can be found by using an information theory-based feature selection algorithm [25]. For this dataset, IC partial areas (IC PA 1 and IC PA 2 defined in Fig. 6) are ranked top two [25] and will be used in this paper. Using the relevance vector regression from [25], models can be built to correlate these selected features with SOH. The relevance vector regression models provide point estimates for SOH, three-sigma (99.7%) credible intervals for estimation uncertainty, and relevance vectors to indicate model complexity.

Table IV summarizes the SOH estimation performance under fast charging with random input SOC ranges for different proposed CNNs. Based on Table IV, virtual IC/DV features extracted from virtual IC/DV curves provide SOH estimation performance that significantly surpasses California’s regulatory requirements (less than 5% SOH estimation error [4]). Furthermore, this SOH performance is similar to that achieved using the same features derived directly from actual IC/DV curves obtained during CC charging. Thus, these virtual IC/DV curves constructed by the proposed U-Net and Mobile U-Net are effective for extending ICA/DVA-based SOH estimation to general charging, which previously could not be done.

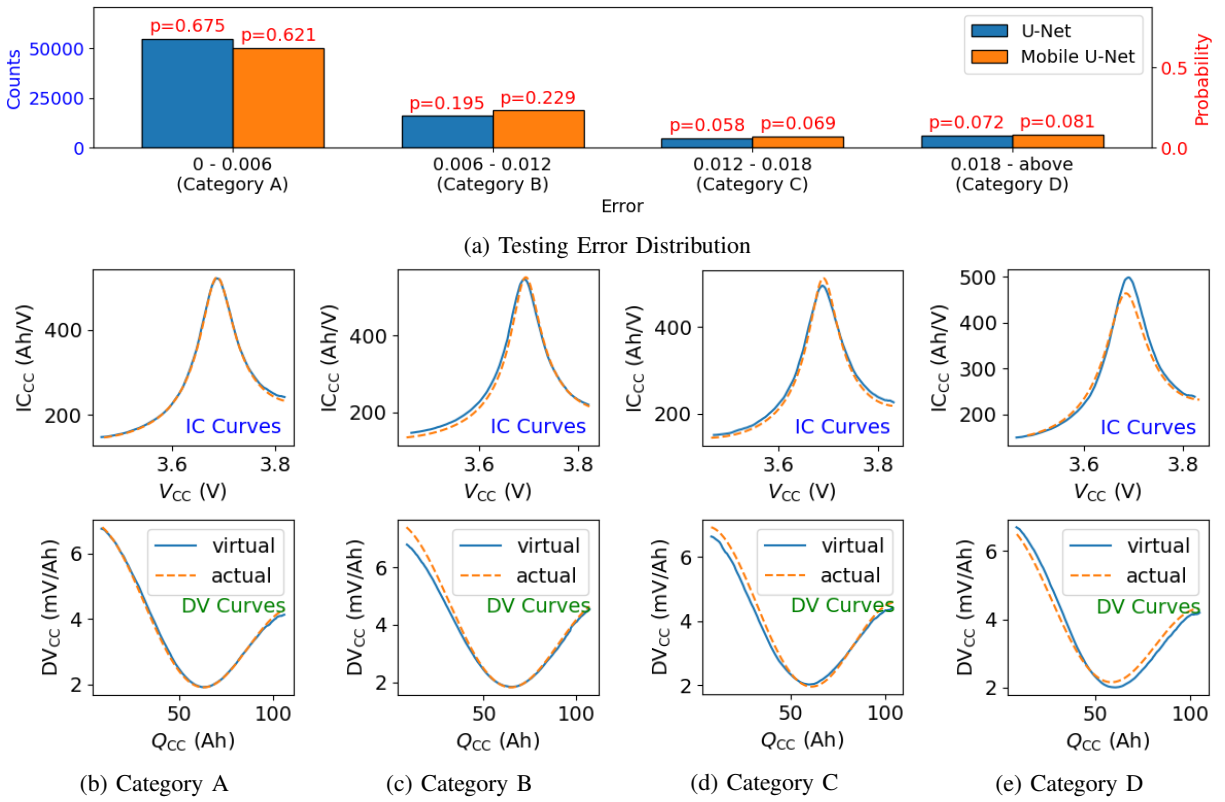


Fig. 7: Performance of Module-Level Virtual IC/DV Curve Construction under Random Input SOC Ranges

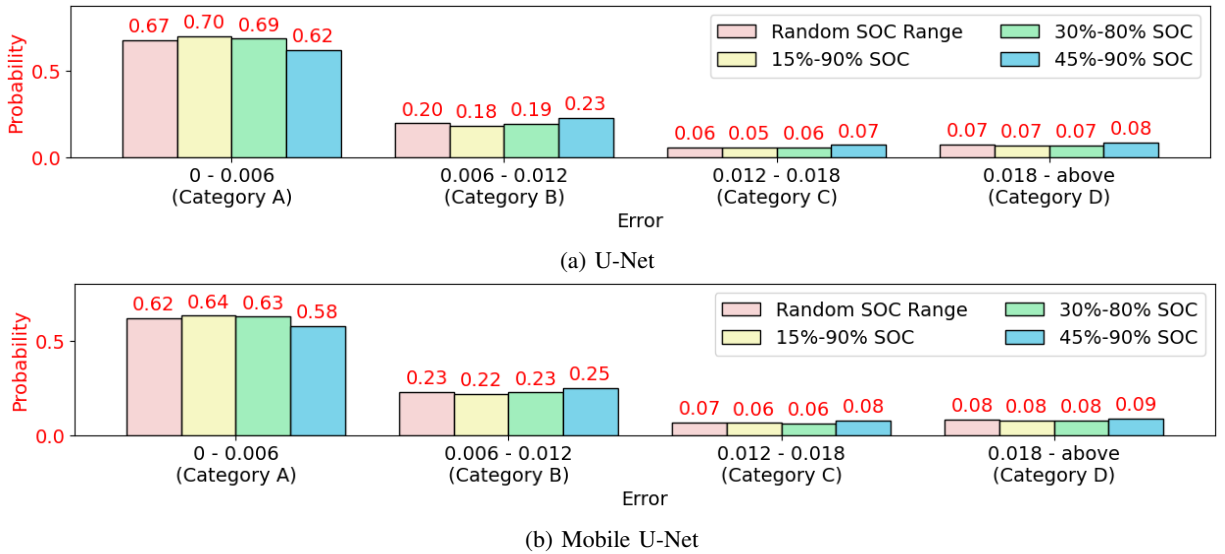


Fig. 8: Testing Error Distributions of Module-Level Virtual IC/DV Curve Construction under Different Input SOC Ranges

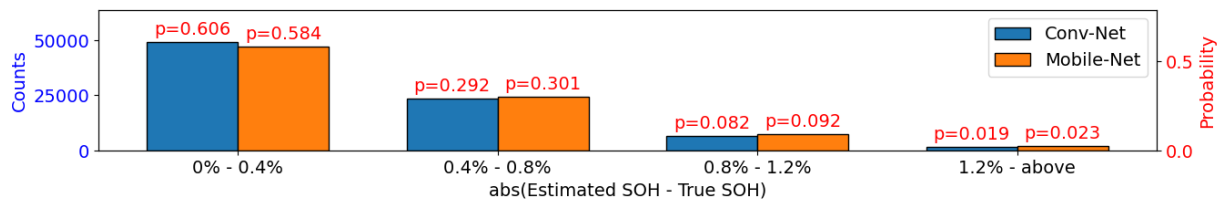


Fig. 9: Testing Absolute SOH Estimation Error Using Conv-Net and Mobile-Net under Random Input SOC Ranges

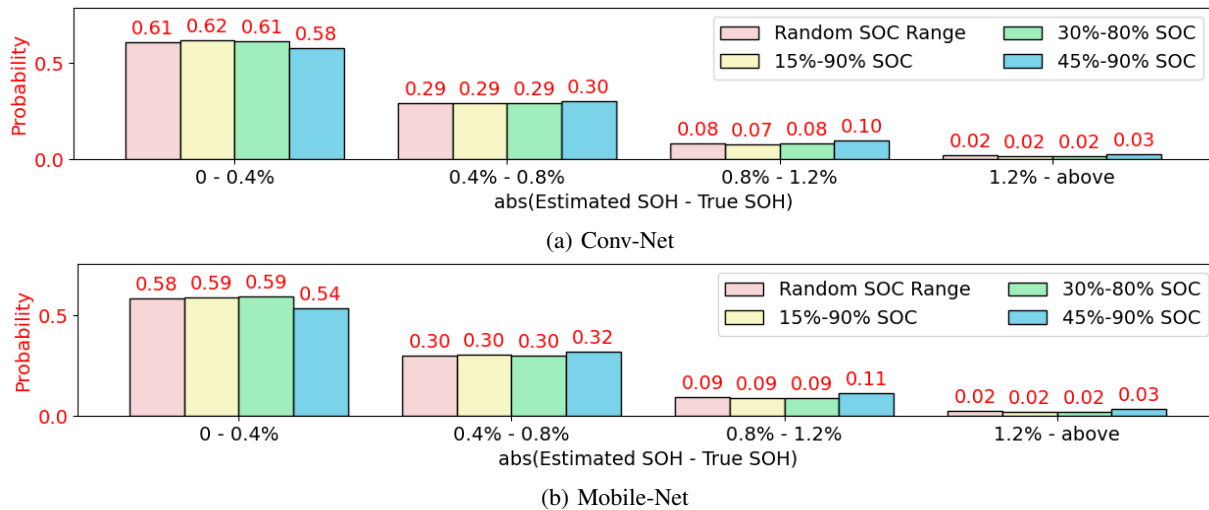


Fig. 10: Testing Absolute Error Distributions for Module-Level SOH Estimation under Different Input SOC Ranges

C. Accuracy of Direct SOH Estimates

When the sole focus is on SOH estimation, the proposed U-Net and Mobile U-Net can be simplified into Conv-Net and Mobile-Net, respectively. This subsection examines and compares the performance of direct SOH estimation using the proposed Conv-Net and Mobile-Net.

Table V summarizes the testing RMSEs for SOH estimation using Conv-Net and Mobile-Net, next to the results obtained from U-Net and Mobile U-Net (discussed in Section VI-B). From Table V, Conv-Net and Mobile-Net provide SOH estimation performance that outperforms virtual IC/DV features and also significantly surpasses California’s regulatory requirements discussed in Section VI-B. Therefore, Conv-Net and Mobile-Net have the advantage of providing better SOH estimation performance, while U-Net and Mobile U-Net provide IC/DV features that can be used for physical interpretations and additional information about battery degradation besides SOH (as discussed in Sections I and II).

TABLE V: SOH Estimation Performance Using Conv-Net and Mobile-Net under Random Input SOC Ranges

Estimation Mode	Neural Network	Test RMSE
Direct Estimation	Conv-Net	0.49% SOH
	Mobile-Net	0.51% SOH
Through Virtual IC/DV Curves	U-Net	0.60% SOH
	Mobile U-Net	0.61% SOH

Fig. 9 shows the testing absolute error distributions for SOH estimation under random input SOC ranges satisfying constraints in Section V-B. Based on Fig. 9 and Table V, one can have the following observations. First, both Conv-Net and Mobile-Net can estimate SOH directly under general charging with good accuracy, while their computation and memory requirements are smaller than other CNNs in the literature as discussed in Section IV. Second, comparing the results between Conv-Net and Mobile-Net, Mobile-Net does not lose too much performance for SOH estimation, but

further reduces the computation and memory (to be discussed in Section VI-D).

To examine how well the Conv-Net and Mobile-Net trained from random input SOC ranges specialize to specific input SOC ranges, the same three cases in Section VI-A are used. Similarly, the proposed Conv-Net and Mobile-Net are not re-trained, and all the data from these 3 cases are used as testing data. Fig. 10 shows the absolute error distributions for the testing set. Based on Fig. 10, the performance of the SOH estimation using Conv-Net and Mobile-Net at specific input SOC ranges stays similar to the random input SOC ranges, but decreases as the input SOC range decreases, because a shorter input SOC range contains less information for SOH estimation.

In summary, the Conv-Net and Mobile-Net trained from random input SOC ranges can be applied directly without re-training for general charging with any specific SOC ranges that meet constraints in Section V-B.

D. Computational Footprint Comparison among Proposed Neural Networks

The computation and memory demands are crucial for onboard implementation feasibility and are directly proportional to the total number of parameters in neural networks. Henceforth, this subsection compares the total number of parameters in the proposed CNNs.

TABLE VI: Number of Parameters in Proposed Convolutional Neural Networks

Models	Total No. of Parameters	No. of Trainable Parameters	No. of Fixed Parameters
U-Net	95503	94323	1180
Mobile U-Net	32425	31385	1040
Conv-Net	73361	12991	60370
Mobile-Net	27118	4946	22172

Table VI summarizes the number of parameters for different proposed CNNs. Based on Table VI, one can have

the following observations. First, most of the parameters in the Conv-Net and Mobile-Net are fixed and inherited from the contraction path of the U-Net and Mobile U-Net for extracting degradation-related features. Second, by comparing U-Net and Mobile U-Net or comparing Conv-Net and Mobile-Net, the mobile versions of the proposed CNNs have only 1/3 of the parameters. Much lower computation and memory demands make them more feasible for onboard implementation. As seen in Sections VI-A, VI-B, and VI-C, with such a significant reduction in the numbers of parameters, the Mobile U-Net and Mobile-Net still maintain good performance for virtual IC/DV curve construction and SOH estimation, compared to the U-Net and Conv-Net.

VII. CONCLUSIONS

This paper proposes a unified approach shown in Fig. 1 and Fig. 3 and, for the first time, makes ICA/DVA-based degradation monitoring feasible under general charging profiles with any SOC ranges that satisfy Constraint (1).

With the concepts of virtual IC/DV curves defined, the proposed U-Net constructs virtual IC/DV curves, which approximate actual IC/DV curves with proven accuracy. SOH estimation is used as a case study to demonstrate the utility of virtual IC/DV curves for degradation monitoring. Applied to a large experimental dataset of NMC622 modules with three parallel-connected cells, virtual IC/DV features achieve 0.60% SOH RMSE and 1.74% average SOH three-sigma value for module-level SOH estimation. The proposed Conv-Net provides accurate SOH estimates directly, if SOH is the only information of interest. For the same dataset, 0.50% SOH RMSE for module-level SOH estimation is achieved. The low demand for computation and memory is the advantage of the proposed Conv-Net over other CNNs in the literature.

The proposed Mobile U-Net and Mobile-Net can replace U-Net and Conv-Net, respectively, to significantly reduce computation and memory requirements for onboard implementations. The mobile versions of the proposed CNNs reduce the number of parameters in CNNs to 1/3 of the original, without losing performance in virtual IC/DV curve construction and SOH estimation. Applied to the same dataset, virtual IC/DV features from Mobile U-Net achieve 0.61% SOH RMSE and 1.77% average SOH three-sigma value for module-level SOH estimation. Mobile-Net achieves 0.51% SOH RMSE for module-level SOH estimation.

Nevertheless, there are some directions for future work. First, a method to determine the minimum required input SOC range for the proposed CNNs to have accurate virtual IC/DV curve construction and SOH estimation needs to be developed. Second, whether the proposed CNNs can work for discharging cases is of interest to be investigated. Third, the effects of measurement noise and vehicle chronometrics on the proposed method will be investigated. Fourth, how to efficiently scale the proposed methods to a large number of modules within a battery pack needs to be researched.

REFERENCES

- [1] A. Barre, B. Deguilhem, S. Grolleau, M. Gerard, F. Suard, and D. Riu, "A review on lithium-ion battery ageing mechanisms and estimations for automotive applications," *Journal of Power Sources*, vol. 241, pp. 680–689, 2013.
- [2] N. Noura, L. Boulon, and S. Jemeï, "A review of battery state of health estimation methods: Hybrid electric vehicle challenges," *World Electric Vehicle Journal*, vol. 11, no. 4, p. 66, 2020.
- [3] M. Bercibar, I. Gandiaga, I. Villarreal, N. Omar, J. V. Mierlo, and P. den Bossche, "Critical review of state of health estimation methods of li-ion batteries for real applications," *Renewable and Sustainable Energy Reviews*, vol. 56, pp. 572–587, 2016.
- [4] "Data standardization requirements for 2026 and subsequent model year light-duty zero emission vehicles and plug-in hybrid electric vehicles," California Code of Regulations, title. 13 § 1962.5.
- [5] B. Philippe, R. Dedryvère, J. Allouche, F. Lindgren, M. Gorgoi, H. Rensmo, D. Gonbeau, and K. Edström, "Nanosilicon electrodes for lithium-ion batteries: Interfacial mechanisms studied by hard and soft x-ray photoelectron spectroscopy," *Chemistry of Materials*, vol. 24, no. 6, p. 1107–1115, 2012.
- [6] P. Abellan, B. L. Mehdı, L. R. Parent, M. Gu, C. Park, W. Xu, Y. Zhang, I. Arslan, J.-G. Zhang, C.-M. Wang, J. E. Evans, and N. D. Browning, "Probing the degradation mechanisms in electrolyte solutions for li-ion batteries by in situ transmission electron microscopy," *Nano Letters*, vol. 14, no. 3, p. 1293–1299, 2014.
- [7] F. Luo, C. Wei, C. Zhang, H. Gao, J. Niu, W. Ma, Z. Peng, Y. Bai, and Z. Zhang, "Operando x-ray diffraction analysis of the degradation mechanisms of a spinel LiMn_2O_4 cathode in different voltage windows," *Journal of Energy Chemistry*, vol. 44, pp. 138–146, 2020.
- [8] L. A. Middlemiss, A. J. Rennie, R. Sayers, and A. R. West, "Characterisation of batteries by electrochemical impedance spectroscopy," *Energy Reports*, vol. 6, pp. 232–241, 2020.
- [9] M. Dubarry, V. Svoboda, R. Hwu, and B. Y. Liaw, "Incremental capacity analysis and close-to-equilibrium ocv measurements to quantify capacity fade in commercial rechargeable lithium batteries," *Electrochemical and Solid-State Letters*, vol. 9, no. 10, p. A454, 2006.
- [10] I. Bloom, A. N. Jansen, D. P. Abraham, J. Knuth, S. A. Jones, V. S. Battaglia, and G. L. Henriksen, "Differential voltage analyses of high-power, lithium-ion cells: 1. technique and application," *Journal of Power Sources*, vol. 139, no. 1-2, pp. 295–303, 2005.
- [11] I. Bloom, J. Christophersen, and K. Gering, "Differential voltage analyses of high-power lithium-ion cells: 2. applications," *Journal of Power Sources*, vol. 139, no. 1-2, pp. 304–313, 2005.
- [12] G. L. Plett, "Extended kalman filtering for battery management systems of lipb-based hev battery packs: Part 3. state and parameter estimation," *Journal of Power Sources*, vol. 134, no. 2, pp. 277–292, 2004.
- [13] G. L. Plett, "Sigma-point kalman filtering for battery management systems of lipb-based hev battery packs: Part 2: Simultaneous state and parameter estimation," *Journal of Power Sources*, vol. 161, no. 2, pp. 1369–1384, 2006.
- [14] S. Schwunk, N. Armbruster, S. Straub, J. Keh, and Matthias Vetter, "Particle filter for state of charge and state of health estimation for lithium-iron phosphate batteries," *Journal of Power Sources*, vol. 239, pp. 705–710, 2013.
- [15] N. Yang, Z. Song, H. Hofmann, and J. Sun, "Robust state of health estimation of lithium-ion batteries using convolutional neural network and random forest," *Journal of Energy Storage*, vol. 48, p. 103857, 2022.
- [16] H. Chaoui and C. C. Ibe-Ekeocha, "State of charge and state of health estimation for lithium batteries using recurrent neural networks," *IEEE Transactions on Vehicular Technology*, vol. 66, no. 10, pp. 8773–8783, 2017.
- [17] C. Weng, Y. Cui, J. Sun, and H. Peng, "On-board state of health monitoring of lithium-ion batteries using incremental capacity analysis with support vector regression," *Journal of Power Sources*, vol. 235, pp. 36–44, 2013.
- [18] A. Krupp, E. Ferg, F. Schuldt, K. Derendorf, and C. Agert, "Incremental capacity analysis as a state of health estimation method for lithium-ion battery modules with series-connected cells," *Batteries*, vol. 7, no. 1, p. 2, 2021.
- [19] X. Pang, X. Liu, J. Jia, J. Wen, Y. Shi, J. Zeng, and Z. Zhao, "A lithium-ion battery remaining useful life prediction method based on the incremental capacity analysis and gaussian process regression," *Microelectronics Reliability*, vol. 127, p. 114405, 2021.

- [20] X. Zhao, J. Wang, M. Zhao, B. Pan, R. Wang, L. Wang, and X. Yan, "Micro-short circuit fault diagnosis of the parallel battery module based on increment capacity curve," *Journal of Energy Storage*, vol. 86, no. A, p. 111201, 2024.
- [21] C. Weng, J. Sun, and H. Peng, "Model parametrization and adaptation based on the invariance of support vectors with applications to battery state-of-health monitoring," *IEEE Transactions on Vehicular Technology*, vol. 64, no. 9, pp. 3908–3917, 2015.
- [22] C. Weng, J. Sun, and H. Peng, "A unified open-circuit-voltage model of lithium-ion batteries for state-of-charge estimation and state-of-health monitoring," *Journal of Power Sources*, vol. 258, no. 9, pp. 228–237, 2014.
- [23] Q. Zhou, E. Hellström, D. Anderson, and J. Sun, "Sensitivity analysis of support vector regression-based incremental capacity analysis for battery state of health estimations," in *2023 IEEE Conference on Control Technology and Applications (CCTA)*, Bridgetown, Barbados, 2023, pp. 1122–1127.
- [24] D. Stephens, Q. Zhou, H. Hofmann, and J. Sun, "Integrated incremental capacity analysis and differential thermal analysis for improved robustness in li-ion battery state of health estimation," in *2024 IEEE Conference on Control Technology and Applications (CCTA)*, Newcastle upon Tyne, UK, 2024, pp. 729–734.
- [25] Q. Zhou, D. Anderson, and J. Sun, "State of health estimation for battery modules with parallel-connected cells under cell-to-cell variations," *eTransportation*, vol. 22, p. 100346, 2024.
- [26] T. Zhang, N. Guo, X. Sun, J. Fan, N. Yang, J. Song, and Y. Zou, "A systematic framework for state of charge, state of health and state of power co-estimation of lithium-ion battery in electric vehicles," *Sustainability*, vol. 13, no. 9, p. 5166, 2021.
- [27] A. Tomaszewska, Z. Chu, X. Feng, S. O'Kane, X. Liu, J. Chen, C. Ji, E. Endler, R. Li, L. Liu, Y. Li, S. Zheng, S. Vetterlein, M. Gao, J. Du, M. Parkes, M. Ouyang, M. Marinescu, G. Offer, and B. Wu, "Lithium-ion battery fast charging: A review," *eTransportation*, vol. 1, p. 100011, 2019.
- [28] X. Tang, Y. Wang, Q. Liu, and F. Gao, "Reconstruction of the incremental capacity trajectories from current-varying profiles for lithium-ion batteries," *Science*, vol. 24, no. 10, p. 103103, 2021.
- [29] C. Wong, A. Weng, S. Pannala, J. Choi, J. B. Siegel, and A. Stefanopoulou, "Differential voltage analysis and patterns in parallel-connected pairs of imbalanced cells," in *2024 American Control Conference (ACC)*, Toronto, Canada, 2024.
- [30] R. Zhou, R. Zhu, C.-G. Huang, and W. Peng, "State of health estimation for fast-charging lithium-ion battery based on incremental capacity analysis," *Journal of Energy Storage*, vol. 51, p. 104560, 2022.
- [31] Y. Chen, L. Torres-Castro, K.-H. Chen, D. Penley, J. Lamb, M. Karulkar, and N. P. Dasgupta, "Operando detection of li plating during fast charging of li-ion batteries using incremental capacity analysis," *Journal of Power Sources*, vol. 539, p. 231601, 2022.
- [32] A. Fly and R. Chen, "Rate dependency of incremental capacity analysis (dq/dv) as a diagnostic tool for lithium-ion batteries," *Journal of Energy Storage*, vol. 29, p. 101329, 2020.
- [33] D. Anseán, V. M. García, M. González, C. Blanco-Viejo, J. C. Viera, Y. F. Pulido, and L. Sánchez, "Lithium-ion battery degradation indicators via incremental capacity analysis," *IEEE Transactions on Industry Applications*, vol. 55, no. 3, pp. 2992–3002, 2019.
- [34] N. Siddique, S. Paheding, C. P. Elkin, and V. Devabhaktuni, "U-net and its variants for medical image segmentation: A review of theory and applications," *IEEE Access*, vol. 9, pp. 82 031–82 057, 2021.
- [35] R. Azad, E. K. Aghdam, A. Rauland, Y. Jia, A. H. Avval, A. Bozorgpour, S. Karimijafarbigloo, J. P. Cohen, E. Adeli, and D. Merhof, "Medical image segmentation review: The success of u-net," *arXiv:2211.14830*, 2022. [Online]. Available: <https://arxiv.org/abs/2211.14830>
- [36] A. G. Howard, M. Zhu, B. Chen, D. Kalenichenko, W. Wang, T. Weyand, M. Andreetto, and H. Adam, "Mobilenets: Efficient convolutional neural networks for mobile vision applications," *arXiv:1704.04861*, 2017. [Online]. Available: <https://doi.org/10.48550/arXiv.1704.04861>
- [37] G. L. Plett, *Battery Management Systems, Volume II: Equivalent-Circuit Methods*. Boston, MA: Artech House, 2015.
- [38] N. Innamorati, T. Ritschel, T. Weyrich, and N. J. Mitra, "Learning on the edge: Investigating boundary filters in cnns," *International Journal of Computer Vision*, vol. 128, p. 773–782, 2020.
- [39] X. Fan, W. Zhang, C. Zhang, A. Chen, and F. An, "Soc estimation of li-ion battery using convolutional neural network with u-net architecture," *Energy*, vol. 256, p. 124612, 2022.
- [40] F. Chollet et al., "Keras," <https://keras.io>, 2015.
- [41] O. Ronneberger, P. Fischer, and T. Brox, "U-net: Convolutional networks for biomedical image segmentation," in *Medical Image Computing and Computer-Assisted Intervention – MICCAI 2015 (MICCAI 2015)*, Munich, Germany, 2015, p. 234–241.
- [42] M. D. Zeiler and R. Fergus, "Visualizing and understanding convolutional networks," in *2014 European Conference on Computer Vision (ECCV)*, Zurich, Switzerland, 2014, pp. 818–833.
- [43] F. Chollet, "Xception: Deep learning with depthwise separable convolutions," in *2017 IEEE Conference on Computer Vision and Pattern Recognition (CVPR)*, Honolulu, USA, 2017, pp. 1800–1807.
- [44] M. Sandler, A. Howard, M. Zhu, A. Zhmoginov, and L.-C. Chen, "Mobilenetv2: Inverted residuals and linear bottlenecks," in *Proceedings of the IEEE Conference on Computer Vision and Pattern Recognition (CVPR)*, Salt Lake City, US, 2018, pp. 4510–4520.
- [45] A. Howard, M. Sandler, G. Chu, L.-C. Chen, B. Chen, M. Tan, W. Wang, Y. Zhu, R. Pang, V. Vasudevan, Q. V. Le, and H. Adam, "Searching for mobilenetv3," in *Proceedings of the IEEE/CVF International Conference on Computer Vision (ICCV)*, Seoul, South Korea, 2019, pp. 1314–1324.
- [46] K. He, X. Zhang, S. Ren, and J. Sun, "Delving deep into rectifiers: Surpassing human-level performance on imagenet classification," in *Proceedings of the IEEE International Conference on Computer Vision (ICCV)*, Santiago, Chile, 2015, pp. 1026–1034.
- [47] S. Ioffe and C. Szegedy, "Batch normalization: Accelerating deep network training by reducing internal covariate shift," in *Proceedings of the 32nd International Conference on Machine Learning*, Lille, France, 2015, pp. 448–456.
- [48] A. Géron, *Hands-on machine learning with Scikit-Learn, Keras, and TensorFlow*. Sebastopol, US: O'Reilly Media, Inc, 2022.
- [49] D. P. Kingma and J. Ba, "Adam: A method for stochastic optimization," *arXiv:1412.6980*, 2017. [Online]. Available: <https://doi.org/10.48550/arXiv.1412.6980>
- [50] X. Gu, K. See, P. Li, K. Shan, Y. Wang, L. Zhao, K. C. Lim, and N. Zhang, "A novel state-of-health estimation for the lithium-ion battery using a convolutional neural network and transformer model," *Energy*, vol. 262, no. B, p. 125501, 2023.
- [51] E. Chemali, P. J. Kollmeyer, M. Preindl, Y. Fahmy, and A. Emadi, "A convolutional neural network approach for estimation of li-ion battery state of health from charge profiles," *Energies*, vol. 15, no. 3, p. 1185, 2022.
- [52] D. Griffin, I. Bate, and R. I. Davis, "Generating utilization vectors for the systematic evaluation of schedulability tests," in *2020 IEEE Real-Time Systems Symposium (RTSS)*, Houston, USA, 2020, pp. 76–88.